Boundary-Layer Meteorol (2007) 122: 517–534
DOI 10.1007/s10546-006-9119-8

ORIGINAL PAPER

The role of surface heterogeneity in modelling the stable boundary layer

A. McCabe · A. R. Brown

Received: 14 February 2006 / Accepted: 28 July 2006 /
Published online: 21 October 2006

Abstract High-resolution numerical simulations are performed for three nights for each of two areas of the United Kingdom. Area-averaging techniques are then used to calculate effective stability functions for turbulence parametrizations in models using typical mesoscale and global spatial resolutions. Comparisons are made with parametrizations commonly used in numerical weather prediction models. The present results do not suggest that significant enhancement of the stability functions above 50 m is justified. Closer to the surface, more significant enhancement is observed in some regions. It is shown that the amount of enhancement is related to the variability of the orography.

Keywords Heterogeneity · Parametrization · Stable boundary layer

1 Introduction

The stable boundary layer over land is typically a nocturnal feature, forming as the daytime heating shuts off and the surface begins to cool. Turbulence driven by wind shear is suppressed by buoyancy forces, resulting in a shallow boundary layer with small-scale eddies. The small scales of these eddies make progress in understanding the stable boundary layer difficult, both in field observations and numerical simulations. In full numerical weather prediction (NWP) models, the stable boundary layer is often so shallow that it is represented by only a few vertical levels. However, adequate representation of the stable layer is important for many aspects of NWP, including forecasting surface temperatures, predicting the timing and the extent of fog formation, and assessing the impact of dispersion events.

It has long been thought that NWP formulations of the stable boundary layer (SBL) have excessive amounts of turbulent mixing compared with that implied by

A. McCabe · A. R. Brown (✉)
Met Office, Fitzroy Road, Exeter EX1 3PB, UK
e-mail: andy.brown@metoffice.gov.uk

observations and large-eddy modelling. This was highlighted by a recent intercomparison of high resolution large-eddy simulations and single column models, conducted as part of the GEWEX (Global Energy and Water Cycle Experiment) Atmospheric Boundary Layer Study, known as GABLS (Beare et al. 2006; Cuxart et al. 2006). All the participating large-eddy models simulated shallower boundary layers with less turbulent mixing than is implied by typical representations of the stable boundary layer in NWP. Alterations to the representation of the stable boundary layer in NWP models, however, have typically resulted in excessive cooling at the surface and a reduction in NWP skill scores (e.g. Viterbo et al. 1999; Beljaars and Viterbo 1998).

One of the possible reasons for needing enhanced mixing in NWP models often suggested is the unresolved heterogeneity at the surface. Mesoscale models are typically run with horizontal resolutions of the order of 10 km, with NWP parametrizations of the turbulent fluxes calculated from mean values over the grid box. These do not take into account localised pockets of mixing occurring on smaller length scales within the grid box, such as might occur with changes in land-use, and local variations in orography. Mahrt (1987) argued that due to the nonlinear relationship between turbulent fluxes and stability, the area-averaged flux of a grid area may differ considerably from the flux calculated from area-averaged variables. Mahrt explores this problem by specifying a Gaussian distribution of Richardson numbers over each grid box, with unity standard deviation and zero mean. His analysis suggests that enhancement of the amount of turbulent mixing is needed for coarser resolution numerical models, but that due to the challenge of making observations in stable regimes, verification of both the spatial distribution of Richardson number, and any implied new formulation of the area-averaged flux, is not always possible. Delage (1997) argued that turbulent fluxes should exist above a critical Richardson number in atmospheric models, due to additional contributions to the turbulent mixing from unresolved variability within a model grid box.

The difference between area-averaged surface fluxes, and the surface flux calculated from area-averaged values is also considered by Acevedo and Fitzjarrald (2003) using observations from a 30 km by 30 km region of complex terrain in New York State, USA. They consider the Louis (1979) formulation of turbulent fluxes, and find that the average surface flux over the region is underestimated for most of the nights considered. To investigate further whether heterogeneity is the real cause of the enhanced mixing needed in NWP models relative to observations and large-eddy model simulations (LES), data are needed at a sufficiently high horizontal resolution over larger areas of mixed terrain. Observations of this form would be the ideal basis for such a study, but difficulties lie in measuring the weak turbulent fluxes in stable conditions, and finding observations of this type over a large enough area and in simple clear sky conditions is not easy.

An alternative approach to using measurements from observational campaigns, is to use data from high resolution NWP models. In the present study, high resolution simulations of the Met Office Unified Model (UM) are used to investigate the role of subgrid surface heterogeneity in the parametrization of turbulent fluxes in the stable boundary layer. A brief description of the choices of parametrization available in the UM is given in Sect. 2. Two locations in the United Kingdom are considered for three separate winter nights, and simulations are run with a horizontal grid length of 1-km with the fluxes parametrized in line with observations and LES, as detailed in Sect. 3. The turbulent fluxes are calculated over grid boxes of coarser mesoscale resolution (i) by area-averaging the 1-km turbulent fluxes, and (ii) from the area-averaged

mean variables. Comparisons of these two values are used to indicate the extent of the additional turbulent mixing needed in mesoscale models to allow for unresolved variability within the grid box.

Of course care has to be taken in interpreting the results of numerical simulations that have limitations themselves. At 1-km resolution the turbulent fluxes within the boundary layer are fully parametrized. However as large-eddy simulation of the stable boundary layer requires resolutions of around 10 m or less (Beare et al. 2006), and is typically run for domains of side of less than 1 km, it is completely computationally unaffordable for the large domains required for the present study.

Recent studies (e.g. Edwards et al. (2006) who used a single column version of the Unified Model) have highlighted how some aspects of the representation of the SBL are sensitive to the details of the turbulence parametrization. However, our assumption is that even if the single column representation of the boundary layer is not perfect, the representation is sufficiently good that a broadly reasonable response to surface heterogeneity can be obtained in a three-dimensional simulation. This is consistent with the approach taken successfully in the past (in a more idealized context) in the development of NWP model parametrizations. For example, simple boundary-layer closure models have been used in the development and evaluation of blending height (e.g. Mason 1988) and orographic roughness length (e.g. Belcher and Wood 1996) parametrization approaches, both of which have proved very useful for NWP models.

Another issue is that in reality there will clearly be heterogeneity (both in terms of orography and surface type) on scales less than 1 km. However, an examination of the impacts of variations on scales larger than 1 km remains a useful step in increasing understanding. Furthermore, arguments can be made (see the discussion in Sect. 4) that shorter scale heterogeneity may have less impact (or at least have an impact restricted to closer to the surface) than that resolved in the present simulations. For these reasons we believe that the approach taken is a valid one, and that the results should represent, at least qualitatively, the impact of heterogeneity on the area-averaged properties of the stable boundary layer.

2 Representation of the stable boundary layer in NWP models

In numerical weather prediction (NWP) schemes, turbulent fluxes of some variable χ are often parametrized by a first-order closure,

$$\overline{w'\chi'} = -K_\chi \frac{\partial \chi}{\partial z}, \tag{1}$$

where K_χ is the eddy diffusivity for χ, w is the vertical velocity, and z is the height above the surface. Different eddy diffusivities may be calculated for momentum, K_m, and for scalar variables, K_h. The difficulty in the parametrization then lies in determining K_m and K_h.

For stable conditions, the current set-up in the Met Office Unified Model (UM) uses a closure based on the local gradient Richardson number, Ri. The diffusivities for momentum and heat are expressed as,

$$K_m = \lambda^2 S f_m(Ri), \tag{2}$$

and,

$$K_h = \lambda^2 S f_h(Ri), \tag{3}$$

where S is the vertical wind shear, λ is a mixing length, and f_m and f_h are stability functions that decay with increasing Richardson number, Ri. The mixing length λ is specified in terms of the height above the surface, the roughness length z_0, von Karman constant κ and asymptotic length scale λ_0 as

$$\frac{1}{\lambda} = \frac{1}{\kappa(z + z_0)} + \frac{1}{\lambda_0}. \tag{4}$$

The eddy diffusivities for momentum and scalars are related through the turbulent Prandtl number, $P_t = K_m/K_h$. The current set-up in the UM is to assume $P_t = 1$ and therefore $f_m(Ri) \equiv f_h(Ri) \equiv f(Ri)$. Historically, changes have been made to the model parametrization by varying the form of these stability functions. One of the many forms available is the 'long-tails' function, which for all $Ri \geq 0$ is given by

$$f_{\text{long-tails}}(Ri) = \frac{1}{1 + 10Ri}. \tag{5}$$

A second is the 'sharp' function of King et al. (2001)

$$f_{\text{sharp}}(Ri) = \begin{cases} (1 - 5Ri)^2 & 0 \leq Ri < 0.1, \\ \left(\dfrac{1}{20Ri}\right)^2 & Ri \geq 0.1. \end{cases} \tag{6}$$

The long-tails function decays more slowly with increasing Richardson number than the sharp function, allowing for more mixing in the stable boundary layer.

Of these two stability functions, the sharp function is widely seen as being the closest to observations and LES, and has been highlighted in the recent GABLS intercomparison of large-eddy models for an idealised stable boundary layer (Beare et al. 2006). In the intercomparison, each of the participating models provided simulations that supported the sharp function over the long-tails. Operationally, however, the long-tails formulation is used in the Met Office global model. Other global modelling centres use a variety of functions (e.g. Louis 1979; Viterbo et al. 1999), the common feature of which is that they give enhanced mixing in stable conditions.

3 Analysis of high resolution numerical simulations

The aim of this work is to use high resolution numerical simulations to investigate whether the reason that NWP models appear to need enhanced mixing in the stable boundary layer relative to observations and LES may be due to unresolved heterogeneity at the surface. With this aim in mind, the Met Office Unified Model is run as a limited area model with 1-km horizontal resolution over two areas of the United Kingdom for three separate winter nights. The simulations are made with the sharp stability function and the asymptotic mixing length, λ_0, set at 40 m. The 1-km data are area-averaged to a typical mesoscale resolution to allow calculation of an adjusted or effective stability function that incorporates the extra variability in the flow resolved by the 1-km simulations. Results from averaging up to a typical global model resolution will also be presented.

3.1 Case studies

Three separate winter nights over the United Kingdom were selected for study: 18–19 November 2004, 15–16 February 2005, and the 27–28 February 2005. The nights were chosen on the basis that the conditions were stable and reasonably clear, so that any variability that was resolved by the model was primarily due to variations at the surface of orography and land type.

For each case, a series of nested simulations was performed. The resolutions varied from approximately 60 km in the global run, through 12 km (on a domain covering much of the Northern Atlantic and Western Europe) and 4 km (over most of the United Kingdom) to 1 km (over two selected areas of the United Kingdom, discussed below). The coarser resolution models provided boundary conditions for the finer resolution ones, and also initial conditions that were reconfigured onto the higher resolution grids. In order to allow for sufficient time for any initial spin-up effects to disappear, the simulations were started several hours before the starts of the nights of interest—at 0900 UTC for the global and 12-km runs, at 1100 UTC for the 4-km runs and at 1300 UTC for the 1-km runs. All simulations ran until 0500 UTC the following day.

The global and 12-km resolution simulations used the standard operational vertical grid, with 38 non-uniformly spaced levels. There were seven levels below 1000 m, with the lowest level at 10 m for winds and at 20 m for potential temperature. However, in order to better resolve the flow near the surface, the 4-km and 1-km resolution simulations were performed with 76 levels in the vertical. These had 10 levels below 500 m, five in the bottom 100 m, and the lowest level at 2.5 m for wind and 5 m for potential temperature. One additional sensitivity test (described in Section 3.3) was performed with still finer resolution near the surface.

For convenience, a summary of the series of simulations performed in each case is given in Table 1; this includes the model timestep and the frequency of calls to the model radiation scheme. Note in particular that the 1-km resolution simulations (on which all analysis is performed) used relatively high frequency calls to the radiation scheme, and that in all simulations this scheme (Edwards and Slingo 1996) was used at full vertical resolution. No subgrid orography or convection parametrizations were used in the 1-km simulations.

The two areas of the United Kingdom for which 1-km resolution simulations were performed are shown in Fig. 1. One of these areas was in southern England, and the other covers the Pennines hill range in the north of England. The southern England area spans 200 km by 144 km, encompassing gentle sloping hills ranging from sea-level to 300 m, and with land-surface types ranging from towns and cities to arable

Table 1 Summary of nested simulations

Resolution (km)	Start time (UTC)	Domain	Timestep (min)	T_{rad} (min)	N_{vert}
60	0900	Global	20	180	38
12	0900	North Atlantic and western Europe	5	60	38
4	1100	Most of UK	1	20	76
1	1300	See Fig. 1	0.13	20	76

T_{rad} is the interval between calls to the model radiation scheme. N_{vert} is the number of vertical levels

Fig. 1 Orography of the southern United Kingdom (as resolved by the 12-km model). Also shown are the domains used by the 1-km resolution simulations. Dotted lines: southern England; dashed lines: Pennines

land. The area over the Pennines covers a slightly larger region of 300 km by 300 km, though some of this is over the sea. Much of the variability at the surface for the northern England region is from the orography that has peaks above 800 m. It should also be noted that some fog was simulated in two of these Pennines simulations—in the low-lying land on both sides of the mountains on the night of 15–16 February 2005, and in a more restricted area to the west of the mountains on the night of 27–28 February 2005.

Results have been analyzed from various times in the nights simulated, but all have been found to be similar in terms of the impact of heterogeneity. Accordingly all results shown will be from the ends of the simulations at 0500 UTC. For each region, a slightly reduced area is considered in order to avoid any problems at the boundaries. Additionally, sea points (which almost exclusively show a convective boundary layer) are excluded from the analysis of the Pennines simulations.

3.2 Variability

For a buoyancy parameter, b, and wind shear, $S = \sqrt{(\partial u/\partial z)^2 + (\partial v/\partial z)^2}$ (where u and v are the horizontal components of wind), the gradient Richardson number can be expressed as

$$Ri = \frac{\partial b/\partial z}{S^2}, \tag{7}$$

The buoyancy gradient is calculated as in Lock et al. (2000), and, in practice, for these largely cloud-free cases, it is closely proportional to the potential temperature gradient.

Figure 2 shows the joint probability distribution function of shear and buoyancy gradient at various levels for the 19 November 2004 case. At 5 m above the surface, a relatively broad distribution of values is seen (although almost all points have $Ri < 0.25$). The higher model levels 'feel' the effects of the surface less, and the variability of shear and buoyancy gradient about their mean values reduces. At the same time, the typical stabilities (as measured by the Richardson number) increase. However, for this case, typical Ri values are still only around 0.5 at 125 m. Note also that the buoyancy gradients (in this and the other cases) are almost exclusively positive. Hence, for these cases, any effect of variability on the area-averaged properties of the boundary layer must arise very largely from changing stability and shear in the stable boundary layer (and not from variability, which forces the boundary layer to be occasionally convective (Mahrt 1987)).

A similar decrease of variability with height was found for the other cases (not shown); however, the different cases do vary somewhat in their stabilities and boundary layer depths (z_i). To illustrate this, Fig. 3 shows distributions of z_i for the modelled stable boundary layer. Here z_i has been defined to be the height of the temperature level immediately below the flux level at which the magnitude of the heat flux first falls below 10% of its surface value. Possible values are the heights of the temperature levels that are indicated on the x-axis of the Figure. For the southern England simulations, the 19 November and 16 February cases show typical z_i values of around 200 m, although the 28 February case is rather more stable and has typical depths of around 80 m. For the Pennines, typical values range from around 300 m in the least stable case (19 November) to only a few tens of metres in the most stable case

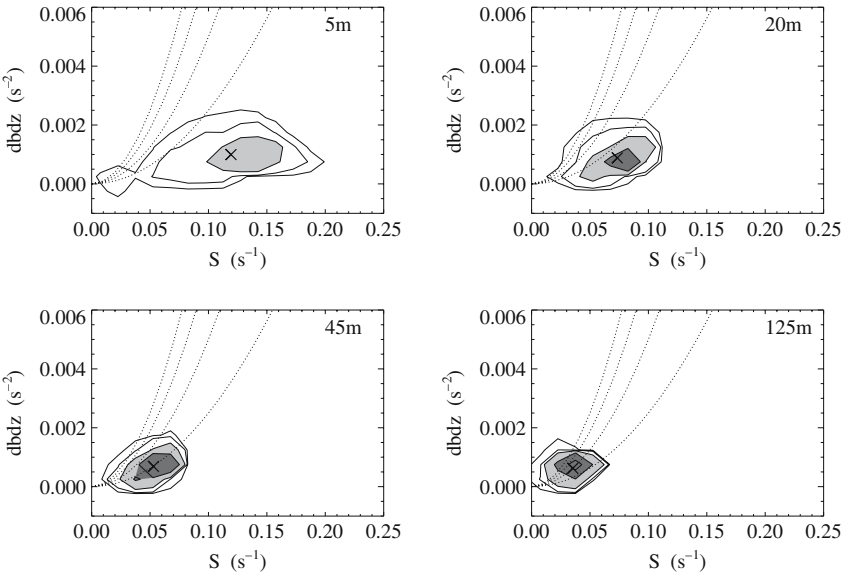

Fig. 2 Joint probability distribution functions of shear (S) and buoyancy gradient ($dbdz$) at various levels at 0500 UTC on the 19 November 2004 from the 1-km resolution southern England simulation. Contours are at (500, 1500, 5000, 15000 and 50000) s^3, with light and dark shading for values over 5000 s^3 and 15000 s^3 respectively. The large cross shows the average values, and the dotted lines show, from left to right, $Ri = 1$, 0.75, 0.5 and 0.25

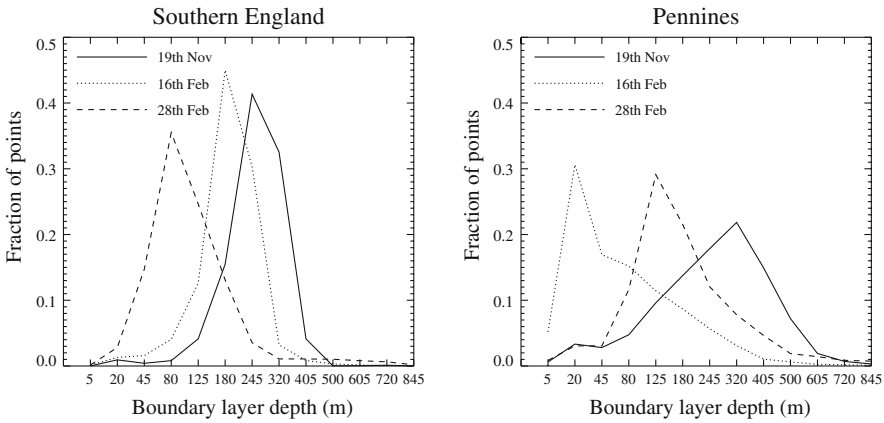

Fig. 3 Distributions of boundary-layer depth (calculated as described in the text)

(16 February). Note that the fact that the boundary layer is not particularly shallow means that they are reasonably well resolved in the vertical. Only the 16 February Pennines case shows significant numbers of points with a boundary layer only two levels deep, and most cases typically have five or more points within the boundary layer.

3.3 Area-averaging to mesoscale model resolution

The Met Office mesoscale model of the United Kingdom currently runs with a resolution of 12 km. In this section, data from the 1-km simulations are used to calculate the turbulent buoyancy fluxes and effective stability functions at mesoscale resolution. Simple arguments using a prescribed idealised variability indicate that considerable variability is needed at 1-km resolution to require a significant enhancement to the effective stability function for a coarser grid model (see Appendix). The primary aim here is to assess whether the variability in the 1-km simulations is sufficient to lead to effective stability functions at 12-km resolution similar to the enhanced mixing formulations often used in NWP.

The buoyancy flux at 12-km resolution is found from the 1-km data in two different ways. The first is by area-averaging the 1-km data to find the mean variables for the buoyancy gradient and wind shear for each grid box, and then calculating the buoyancy flux for the 12-km grid box using the parametrization given in Eq. (1). This gives the average buoyancy flux on the 12-km grid box, $\overline{wb}_{12}$, as

$$\overline{wb}_{12} = \langle\lambda\rangle^2 \langle S\rangle \left\langle \frac{\partial b}{\partial z} \right\rangle f(\langle Ri\rangle), \tag{8}$$

where $\langle\rangle$ denotes the average over the 12-km grid box, $\langle S\rangle = \sqrt{\langle \partial u/\partial z\rangle^2 + \langle \partial v/\partial z\rangle)^2}$, and $\langle Ri\rangle = \langle \partial b/\partial z\rangle / \langle S\rangle^2$. This is the flux a coarser resolution model may be expected to have, using the standard stability functions.

The second method for calculating the buoyancy flux at 12 km incorporates the flux at each individual 1-km grid point. The same formula as above is used to calculate the 1-km buoyancy flux, $\overline{wb}_1$, as,

$$\overline{wb}_1 = \lambda^2 S \frac{\partial b}{\partial z} f(Ri), \tag{9}$$

at each grid point. Then the buoyancy flux for the 12-km grid box incorporating the 1-km heterogeneity, $\overline{wb}_{\text{het}}$, is the average of these 1 km fluxes, i.e.,

$$\overline{wb}_{\text{het}} = \langle wb_1 \rangle . \tag{10}$$

This buoyancy flux can also be written in terms of the area-averaged mean variables as

$$\overline{wb}_{\text{het}} = \langle \lambda \rangle^2 \langle S \rangle \left\langle \frac{\partial b}{\partial z} \right\rangle f_{\text{het}}(\langle Ri \rangle), \tag{11}$$

where f_{het} is an effective stability function that incorporates the heterogeneity at 1 km. Re-arranging, the effective stability function, f_{het}, can then be expressed as,

$$f_{\text{het}}(\langle Ri \rangle) = \frac{\overline{wb}_{\text{het}}}{\overline{wb}_{12}} f(\langle Ri \rangle), \tag{12}$$

defined at each of the 12-km grid boxes.

Figure 4 shows the effective stability function f_{het} for each 12-km grid point as it varies with the area-averaged gradient Richardson number for all three nights at both locations. The three curves included on the plots are the sharp, Louis, and Long-tails functions. The long-tails and sharp functions are defined in Eqs. (5) and (6) respectively; the Louis function, f_{louis}, is defined as (Louis 1979),

$$f_{\text{louis}} = \frac{1}{(1 + 5Ri)^2}, \tag{13}$$

and lies between the sharp and long-tails functions. The plots show the effective stability function at three categories of height: 5 m, 20 m and 45 m and 80 m, corresponding to the lowest two model levels, and to levels three and four together.

The extent to which the effective stability function, f_{het}, differs from the sharpest function varies depending on both the area and the night considered. For southern England, there is virtually no difference between f_{het} and f_{sharp} for the 19 November case. For the more stable cases of 16 February and 28 February, rather more enhancement of f_{het} is seen at the lowest model level, although the majority of points still lie below f_{louis}. At higher levels the diagnosed enhancements are typically very small, with almost all of the points lying close to (but usually just above) f_{sharp}.

For the Pennines simulations, the differences between f_{het} and f_{sharp} are generally rather larger. At the lowest model level the enhancements are often quite large, so that a significant number of points have f_{het} larger than f_{louis} or even $f_{\text{long-tails}}$. This is particularly noticeable in the most stable of the cases (16 February). As in the southern England simulations, the impact of heterogeneity reduces at higher levels and the values of f_{het} are almost always less than f_{louis} at 20 m and above. However, unlike in the southern England simulations, a considerable number of points do remain significantly above f_{sharp} i.e. the impact of heterogeneity is not confined to the lowest grid level. This is particularly noticeable in the 19 November and 28 February cases. In the 16 February case the increases of f_{het} above f_{sharp} at the higher levels are generally smaller, presumably because these levels are typically more stable (or even above the boundary-layer top) in this case.

Noting that largest enhancements of f_{het} above f_{sharp} occur at the lowest model level, an extra test was carried out to check that these relatively large enhancements

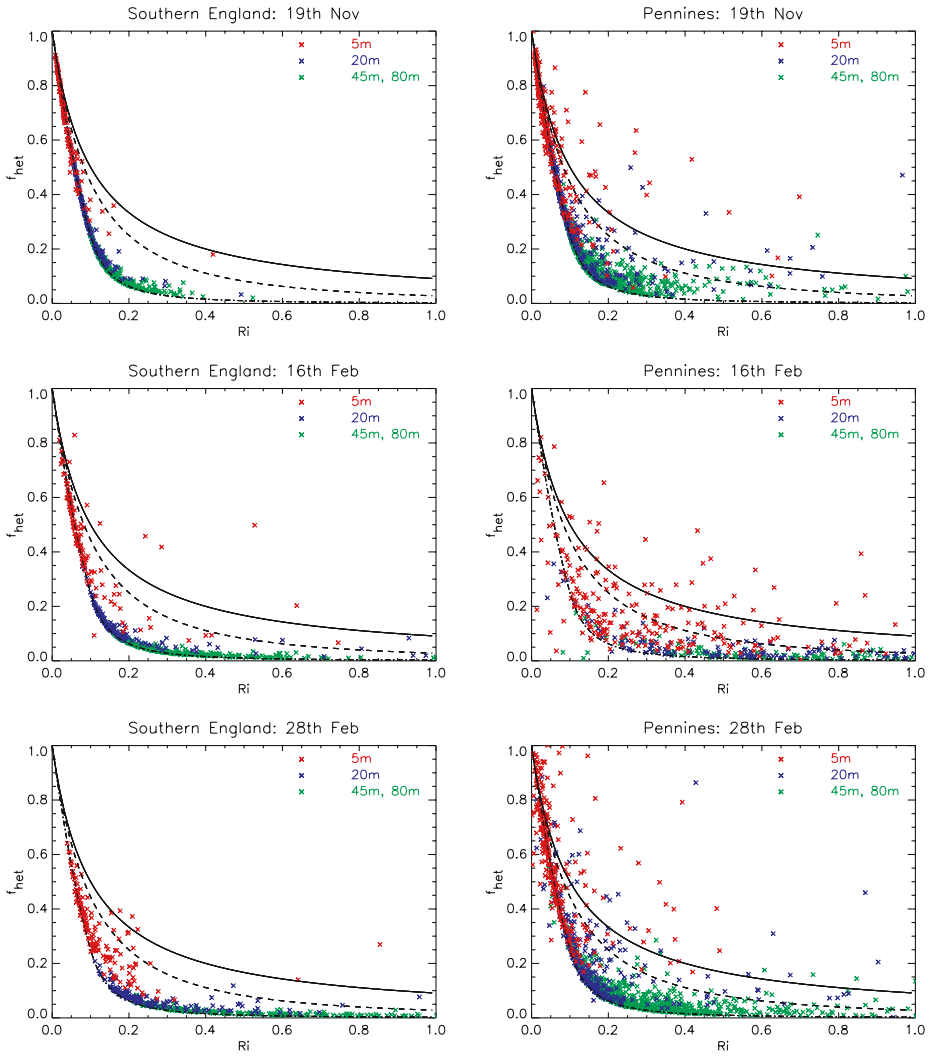

Fig. 4 Effective stability function for 12-km grid boxes, f_{het}, as a function of the gradient Richardson number. Results are shown at 5 m, at 20 m, and at 45 m and 80 m. The left-hand column shows results from the southern England limited area, and the right-hand column from the Pennines area. Results from the different nights are shown in the three rows. The curves plotted on each panel are, reading from top to bottom, $f_{\mathrm{long\text{-}tails}}$, f_{louis} and f_{sharp}, although the f_{sharp} curve, lying close to the bottom edge of the main mass of symbols, is often obscured

were not some artefact of the model lower boundary condition. To investigate this, the 19 November Pennines case was rerun with the vertical resolution doubled again in the lower boundary layer—hence lowest potential temperature levels (at which f_{het} is diagnosed) at 2.5 m, 5 m, 12.5 m and 20 m. Encouragingly, plots (not shown) of f_{het} versus Ri at 5 m and 20 m (now the second and fourth model levels) were found to be very similar to those obtained in the standard runs in which these were the lowest two model levels. This suggests that the results are robust.

Figure 5 shows contour plots of the orography of the 1-km simulations. The symbols show into which of the four categories the value of f_{het} at 5 m for the 28 February case falls:

(i) $f_{\text{het}} \leq 0.67 f_{\text{sharp}} + 0.33 f_{\text{louis}}$,
(ii) $0.67 f_{\text{sharp}} + 0.33 f_{\text{louis}} < f_{\text{het}} \leq f_{\text{louis}}$,
(iii) $f_{\text{louis}} < f_{\text{het}} \leq f_{\text{long-tails}}$, and
(iv) $f_{\text{het}} > f_{\text{long-tails}}$.

For southern England, the majority of the points lie in category (i) i.e. little or no increase in mixing relative to the sharp function. Of the remaining points, most are in category (ii), with relatively few in categories (iii) and (iv). There is a suggestion that the points with most enhanced mixing tend to be in the regions of significant orographic variability (e.g. in the west and centre of the area). A similar impression was gained from examination of the results for other nights (not shown). The Pennines area results are more convincing in highlighting the importance of orography in generating extra mixing. Many of the points in the significantly orographic regions lie in category (iv), while those away from orography lie mainly in category (i).

In order to further illustrate the relationship between orography and enhanced mixing, Fig. 6 shows f_{het} (all three Pennines cases combined) as a function of the 12-km grid-box average Richardson number separately (at two heights) for four different ranges of the standard deviation of orography (σ) within the grid box. The latter was used, rather than mean orographic height, as it seems more likely to relate to the variability. Although there is considerable scatter, a tendency to greater values of f_{het} as σ increases can be seen, both at 5 m and 45 m. For example, at 5 m, most of the boxes with $\sigma < 20$ m have $f_{\text{het}} < f_{\text{louis}}$, while boxes with $\sigma > 100$ m mainly have $f_{\text{het}} > f_{\text{long-tails}}$. At 45 m, the enhancements above f_{sharp} are, as previously noted, smaller. With $\sigma \lesssim 50$ m very little enhancement is seen. With larger values of σ, the enhancements are more significant, although even with $\sigma > 100$ m nearly all of the boxes have $f_{\text{het}} < f_{\text{long-tails}}$ and most have $f_{\text{het}} < f_{\text{louis}}$.

3.4 Area-averaging to global model resolution

In order to allow a wider range of scales to contribute to the variability, the preceding analysis has been repeated, but this time averaging over boxes of side 40 km. This is of interest as global NWP models typically run with resolutions of a few tens of kilometres. However, the results have been found to be qualitatively very similar to those obtained when averaging over 12-km boxes. To illustrate this, Fig. 7 is exactly as Fig. 6, except with the diagnosis now made over 40-km square boxes. Inevitably there are many fewer points than in Fig. 6, and the larger boxes are less likely to show very small values of orographic standard deviation. Nevertheless, the distributions of points are broadly similar to those in Fig. 6, again showing the enhancement of f_{het} above f_{sharp} tending to increase with increasing σ, but decreasing with increasing height above the surface (so that at 45 m the diagnosed f_{het} is typically close to f_{sharp} and only approaches f_{louis} in the boxes with the largest values of σ).

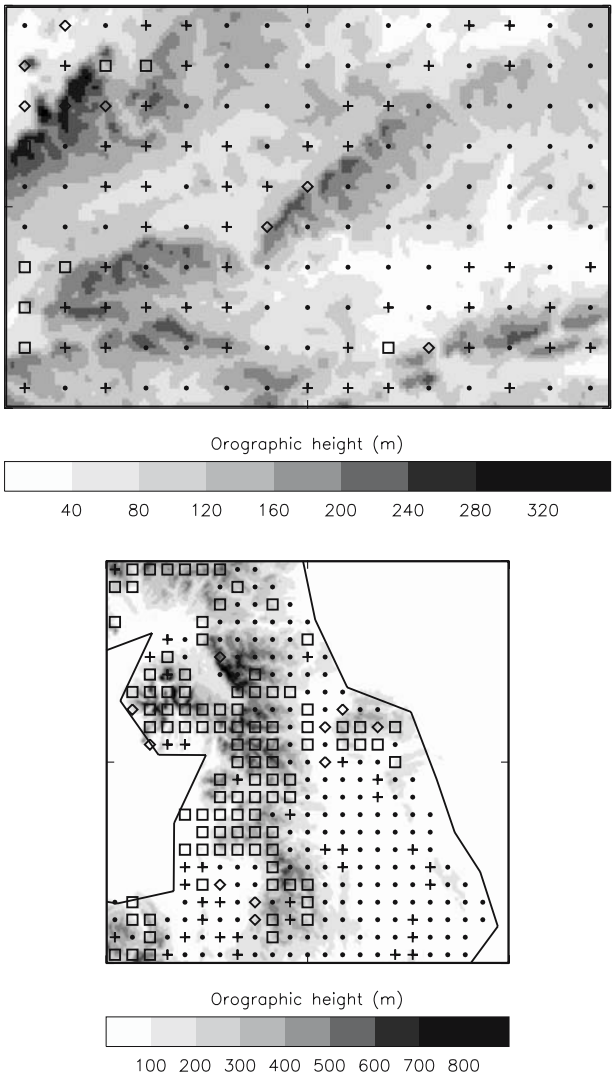

Fig. 5 Plots of 1-km orography for (top) southern England and (bottom) Pennines area. The symbols give an indication of the value of f_{het} at 5 m for the 28 February case for each 12-km grid square: · : category (i); + : category (ii); ◇ : category (iii); □ : category (iv). No symbol is plotted if the Richardson number based on the averaged fields is negative

Fig. 6 Effective stability function for 12 km grid boxes, f_{het}, as a function of the gradient Richardson ▶ number from the Pennines simulations (all three cases combined). The left and right columns show results obtained at two different heights (5 m and 45 m) and the different rows show results restricted to 12-km boxes with orographic standard deviation (σ) within the box falling within various ranges (< 20 m, 20–50 m, 50–100 m and > 100 m). The curves plotted on each panel are, reading from top to bottom, $f_{\text{long-tails}}$, f_{louis} and f_{sharp}

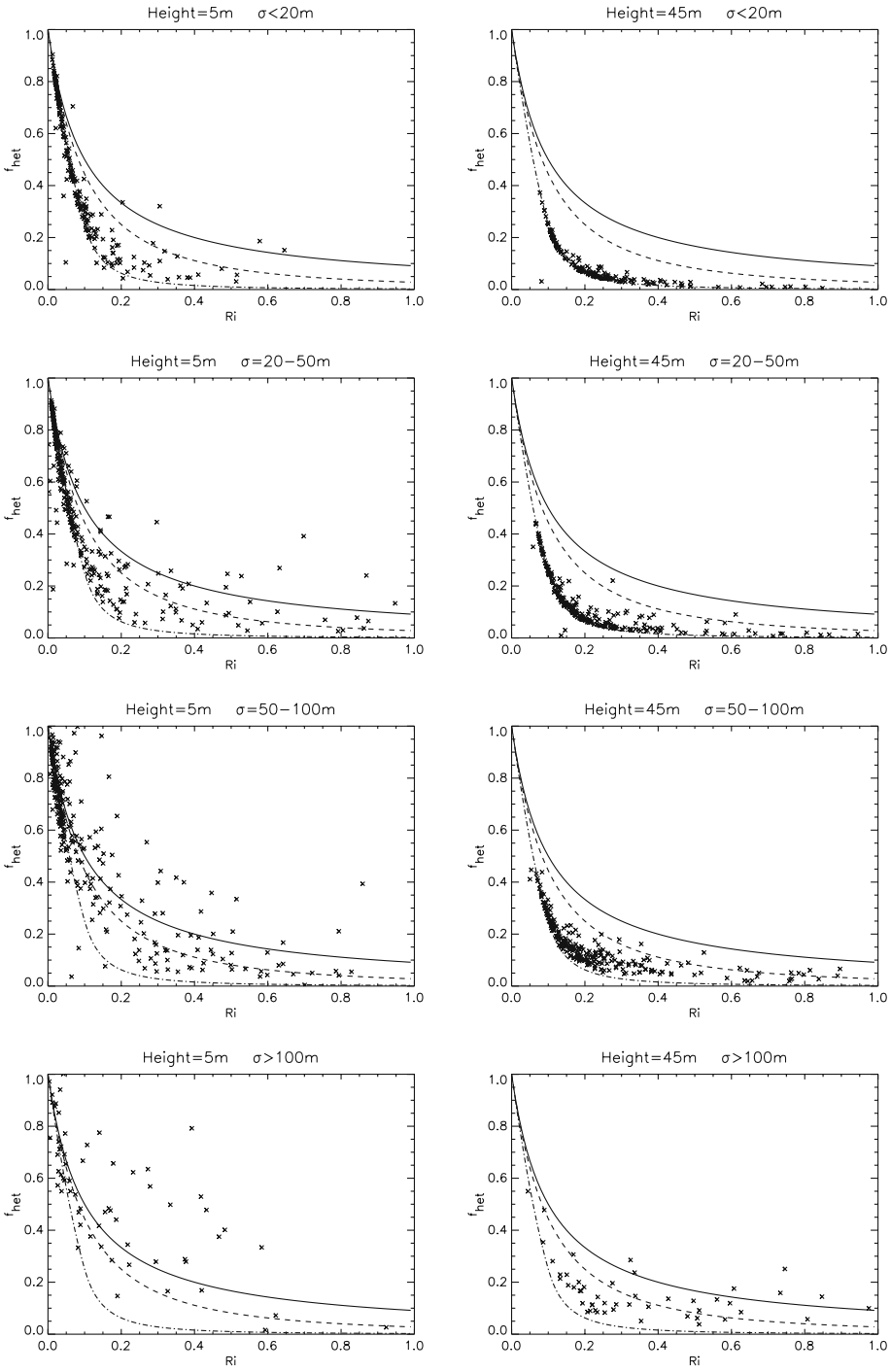
Height=5m σ<20m
Height=45m σ<20m
Height=5m σ=20−50m
Height=45m σ=20−50m
Height=5m σ=50−100m
Height=45m σ=50−100m
Height=5m σ>100m
Height=45m σ>100m
f_het
Ri
0.0
0.2
0.4
0.6
0.8
1.0

Fig. 7 Effective stability function for 40-km grid boxes, f_{het}, as a function of the gradient Richardson number from the Pennines simulations (all three cases combined). The left and right columns show results obtained at two different heights (5 m and 45 m) and the different rows show results restricted to 40-km boxes with orographic standard deviation (σ) within the box falling within various ranges (< 20 m, 20–50 m, 50–100 m and > 100 m). The curves plotted on each panel are, reading from top to bottom, $f_{\text{long-tails}}$, f_{louis} and f_{sharp}

4 Discussion

The 12-km and 40-km results presented are based on numerical simulations that, of course, have their limitations. The real world will have significant variability on scales shorter than 1 km (and the 1-km simulations will themselves underestimate variability on scales of a few kilometres due to numerical diffusion and the smoothing of orography). However, it is difficult to see how this still unresolved variability could lead to the need for significantly enhanced mixing well above the surface. Theory for flow over hills (Belcher et al. 1993) (and also flow over varying roughness (Belcher et al. 1990)) suggests that there should not be significant turbulent flux perturbations in the outer region, where rapid distortion dynamics are applicable. Taking the neutral estimate of the inner region depth (and hence for the height of the base of the outer region) gives, for a roughness length of 0.1 m, 40 m for a surface variation of wavelength 3 km, 16 m for a wavelength of 1 km and 6 m for a wavelength of 300 m. This suggests that none of these scales, and in particular not the shorter scales unresolved in the 1-km simulations, should be expected to significantly influence directly the area-averaged transfer efficiency above 50 m.[1] Significant velocity perturbations due to drainage currents on short-scale hills are also not expected to extend more than a few tens of metres above the surface (Atkinson 1995). It is also worth noting that, for a given flow variability, a first-order turbulence scheme (as used in the UM) will tend to *overestimate* rather than underestimate turbulent flux perturbations in the outer region. One effect that could conceivably lead to enhanced mixing aloft would be the breaking of gravity waves triggered by small-scale orography, but the importance of this mechanism in reality is unclear. Assuming that it is not a dominant effect, the lack of large enhancements to the effective stability functions above 50 m or so seems theoretically reasonable, and likely to be robust to the inclusion of variability on smaller scales.

5 Summary and conclusions

In this study high resolution numerical simulations have been used to investigate the role of surface heterogeneity in the stable boundary layer. Three separate winter nights have been considered over two areas of the United Kingdom. Area-averaging techniques were used to diagnose effective stability functions for typical mesoscale and global horizontal resolutions. Comparisons were made between the effective stability function and some enhanced mixing formulations used in NWP models.

The amount of enhancement to the mixing has been shown to be related to the variability of the orography. For southern England, where the orography is relatively

[1] There may be an indirect effect on the momentum transfer if the pressure drag on hills is significant. However, at least in principle, this effect is typically taken into account through the subgrid orographic parametrization (e.g. by the use of effective roughness lengths).

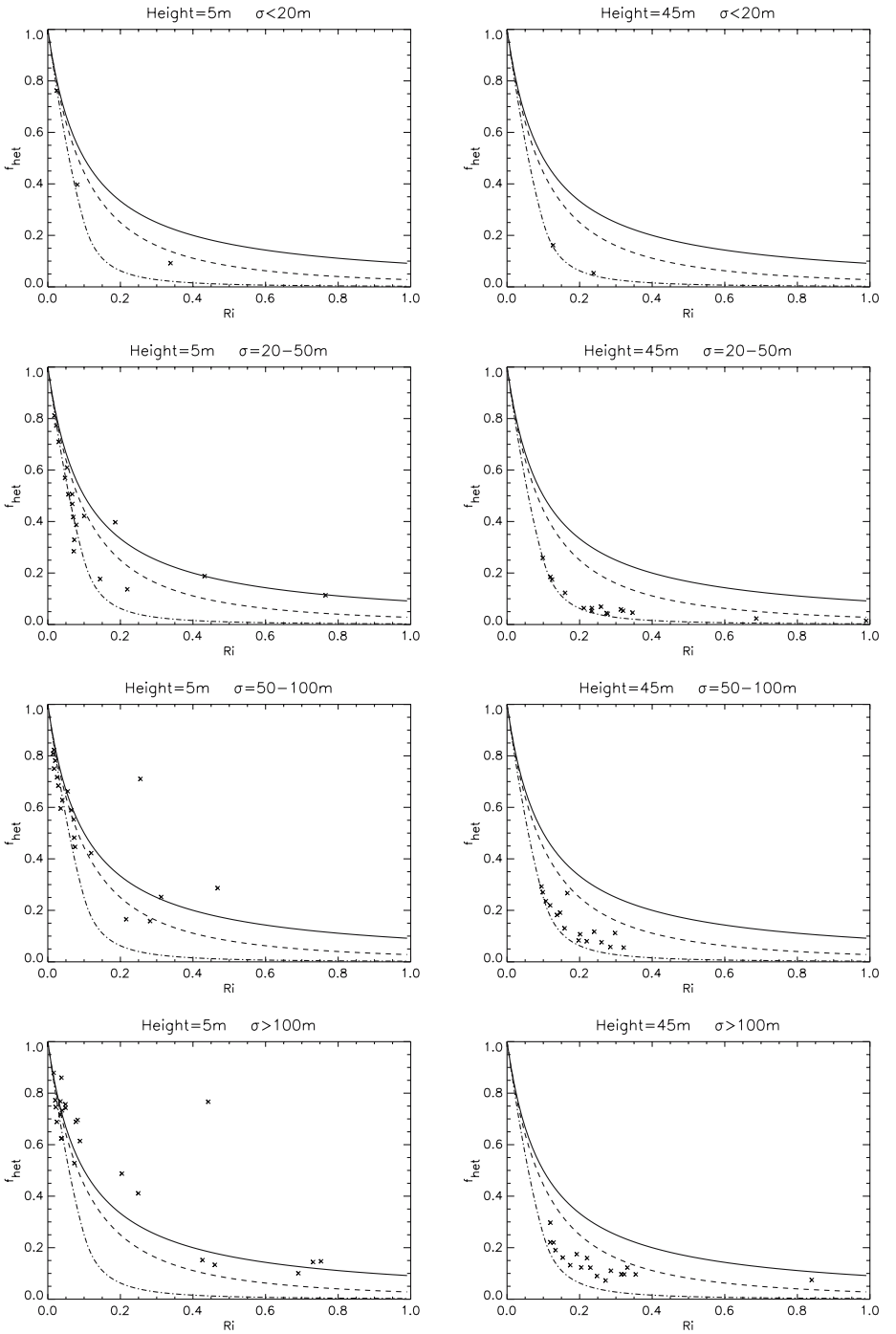
Height=5m σ<20m
Height=45m σ<20m
Height=5m σ=20−50m
Height=45m σ=20−50m
Height=5m σ=50−100m
Height=45m σ=50−100m
Height=5m σ>100m
Height=45m σ>100m
f_het
Ri
0.0
0.2
0.4
0.6
0.8
1.0

gentle, the effective stability function for most mesoscale model grid boxes is not much enhanced from the sharp function (although a tendency for stronger mixing close to the surface can be ascertained in the more hilly regions). The Pennines domain in northern England contains regions of much more significant orography. At 5 m above the surface, a significant number of 12-km and 40-km grid boxes show effective stability functions in excess of those given by f_{louis} and even $f_{\text{long-tails}}$. However, the effects of variability decrease with height, and even for the Pennines area only a few grid boxes show mixing enhanced to anything approaching f_{louis} for heights above 50 m.

These results suggest that the effects of heterogeneity on scalar mixing are not large enough to justify general use of functions (e.g. f_{louis} and $f_{\text{long-tails}}$) that give significantly enhanced mixing at all heights. However, a case could be made for allowing enhanced mixing close to the surface where the effects of heterogeneity on the effective mixing coefficient are more significant. In fact, something in this spirit is currently done in the operational Met Office mesoscale model, where a match is made between an enhanced mixing function at the surface (Beljaars and Holtslag (1991) in the surface transfer coefficient and f_{louis} in the boundary-layer mixing scheme) and f_{sharp} at 200 m and above. However, the present results suggest that the transition of the function towards f_{sharp} should occur rather more quickly as distance from the surface increases. At the coarser operational vertical resolution, the most significant enhancement would be represented through the surface transfer coefficient (rather than through the eddy diffusivity used within the boundary layer). However, the present results suggest that, rather than using the same enhanced function everywhere at the surface, it would be more appropriate to make the enhancement above f_{sharp} a function of the orographic variability. Any weak effects of variability of land-surface type are probably already accounted for through the use of tiling schemes, which perform separate surface transfer calculations for each type of surface.

Appendix

By assuming simple distributions of shear and buoyancy gradient, it is possible to obtain an idea of how much variability is required in order to produce effective heat transfer stability functions (f_{het}) for the area-averaged fields that differ significantly from the local functions (f). For example, taking $f = 1/(20Ri)^2$ (the 'sharp' function that is used in the model for $Ri > 0.1$), writing the shear (S) and buoyancy gradient (b_z) as the sum of mean and perturbation parts, using Eqs. (8)–(12) and rearranging leads to

$$f_{\text{het}}(\overline{Ri}) = f(\overline{Ri}) \overline{\left[\frac{\left(1 + \frac{S'}{\overline{S}}\right)^5}{\left(1 + \frac{b'_z}{\overline{b_z}}\right)} \right]}. \tag{A1}$$

Expanding and retaining only terms up to second order in perturbation quantities then leads to

$$f_{\text{het}}(\overline{Ri}) \simeq f(\overline{Ri}) \left[1 + 10\overline{\left(\frac{S'}{\overline{S}}\right)^2} + \overline{\left(\frac{b'_z}{\overline{b_z}}\right)^2} - 5\overline{\left(\frac{S'}{\overline{S}}\right)\left(\frac{b'_z}{\overline{b_z}}\right)} \right] \tag{A2}$$

It can be seen from this equation that variability in normalized shear ($S'/\overline{S}$) is much more effective than variability in normalized buoyancy gradient ($b'_z/\overline{b_z}$) in increasing

$f_{\rm het}$ above f. This relatively strong dependence on the shear variability arises primarily from the dependence of f on the Richardson number, which itself depends on the square of the shear. Nevertheless, considerable variability of shear is required in order to have a significant impact on $f_{\rm het}$, particularly at larger Richardson numbers. For example, considering a case with no buoyancy gradient perturbations, but with a Gaussian distribution of shears with standard deviation of 40% of the mean value, Eq. (A1) predicts $f_{\rm het} = 3.05f$. At $\overline{Ri} = 0.2$ (for which $f = 0.06$) this gives $f_{\rm het} = 0.19$, which is reasonably close to $f_{\rm louis} = 0.25$ and $f_{\rm long\text{-}tails} = 0.33$. However, at $\overline{Ri} = 0.5$ (for which $f = 0.01$), $f_{\rm het} = 0.03$ while $f_{\rm louis} = 0.08$ and $f_{\rm long\text{-}tails} = 0.16$. These arguments therefore suggest that a very large variability of shear would be required in order to make $f_{\rm het}$ approach the values given by parametrizations ($f_{\rm long\text{-}tails}$ in particular) at high stabilities.

Although the focus of our study is on the effective stability function for scalar mixing, it is easy to perform a similar calculation to obtain that ($f_{\rm het}^{\rm mom}$) for momentum mixing (with the analogues to Eqs. (8), (9) and (11) containing an extra factor of shear replacing the buoyancy gradient). This leads to

$$f_{\rm het}^{\rm mom}(\overline{Ri}) = f(\overline{Ri}) \overline{\left[\frac{\left(1 + \frac{S'}{\overline{S}}\right)^6}{\left(1 + \frac{b'_z}{\overline{b_z}}\right)^2} \right]}$$
$$\simeq f(\overline{Ri}) \left[1 + 15\overline{\left(\frac{S'}{\overline{S}}\right)^2} + 3\overline{\left(\frac{b'_z}{\overline{b_z}}\right)^2} - 12\overline{\left(\frac{S'}{\overline{S}}\right)\left(\frac{b'_z}{\overline{b_z}}\right)} \right]. \qquad \text{(A3)}$$

Hence variability in shear and buoyancy gradient is expected to have an impact on area-averaged momentum mixing that is qualitatively similar to that on scalar mixing (although with some quantitative differences).

References

Acevedo OC, Fitzjarrald DR (2003) In the core of the night–effects of intermittent mixing on a horizontally heterogeneous surface. Boundary-Layer Meteorol 106:1–33

Atkinson BW (1995) Orographic and stability effects on valley-side drainage flows. Boundary-Layer Meteorol 75:403–428

Beare RJ, MacVean MK, Holtslag AAM, Cuxart J, Esau I, Golaz J-C, Jimenez MA, Khairoutdinov M, Kosovic B, Lewellen D, Lund TS, Lundquist JK, McCabe A, Moene AF, Noh Y, Raasch S, Sullivan P (2006) An intercomparison of large-eddy simulations of the stable boundary layer. Boundary Layer Meteorol 118:247–272

Belcher SE, Newley TMJ, Hunt JCR (1993) The drag on an undulating surface induced by the flow of a turbulent boundary layer. J Fluid Mech 249:557–596

Belcher SE, Wood N (1996) Form and wave drag due to stably stratified flow over low ridges. Quart J Roy Meteorol Soc 122:863–902

Belcher SE, Xu DP, Hunt JCR (1990) The response of a turbulent boundary layer to arbitrarily distributed two-dimensional roughness changes. Quart J Roy Meteorol Soc 116:611–635

Beljaars ACM, Holtslag AAM (1991) Flux parametrization over land surfaces for atmospheric models. J Appl Meteorol 30:327–341

Beljaars ACM, Viterbo P (1998) Role of the boundary layer in a numerical weather prediction model. In: Holtslag AAM, Duynkerke PG (eds) Clear and Cloudy Boundary Layers, Royal Netherlands Academy of Arts and Sciences, Amsterdam, pp 287–304

Cuxart J, Holtslag AAM, Beare RJ, Bazile E, Beljaars A, Cheng A, Conangla L, Ek M, Freedman F, Hamdi R, Kerstein A, Kitagawa H, Lenderink G, Lewellen D, MAilhot J, Mauritsen T, Perov V, Scheyes G, Steenveld GJ, Svensson G, Taylor P, Weng W, Wunsch S, Xu KM (2006) Single-column

model intercomparison for a stably stratified atmospheric boundary layer. Boundary Layer Meteorol 118:273–303
Delage Y (1997) Parameterising sub-grid scale vertical transport in atmospheric models under statically stable conditions. Boundary-Layer Meteorol 82:23–48
Edwards JM, Beare RJ, Lapworth AJ (2006) Simulation of the observed evening transition and nocturnal boundary layers: single-column modelling. Quart J Roy Meteorol Soc 132:61–80
Edwards JM, Slingo A (1996) Studies with a flexible new radiation code. I: choosing a configuration for a large-scale model. Quart J Roy Meteorol Soc 122:689–719
King JC, Connolley WM, Derbyshire SH (2001) Sensitivity of modelled Antarctic climate to surface and boundary-layer flux parametrizations. Quart J Roy Meteorol Soc 127:779–794
Lock AP, Brown AR, Bush MR, Martin GM, Smith RNB (2000) A new boundary layer mixing scheme. part I: Scheme description and single-column model tests. Mon Wea Rev 128:3187–3199
Louis J-F (1979) A parametric model of vertical eddy fluxes in the atmosphere. Boundary-Layer Meteorol 17:187–202
Mahrt L (1987) Grid-averaged surface fluxes. Mon Wea Rev 115:1550–1560
Mason PJ (1988) The formation of areally-averaged roughness lengths. Quart J Roy Meteorol Soc 114:399–420
Viterbo P, Beljaars ACM, Mahouf J-F, Teixeira J (1999) The representation of soil moisture freezing and its impact on the stable boundary layer. Quart J Roy Meteorol Soc 125:2401–2426